

# Deformation mechanism in a twin-roll cast AA5754 alloy

P. Málek<sup>1\*</sup>, K. Turba<sup>1</sup>, M. Slámová<sup>2</sup>

<sup>1</sup>Charles University, Faculty of Mathematics and Physics, Department of Physics of Materials, Ke Karlovu 5, CZ-121 16 Prague 2, Czech Republic

<sup>2</sup>Research Institute for Metals, Ltd., Panenské Břežany, 250 70 Odolena Voda, Czech Republic

Received 29 May 2008, received in revised form 8 July 2008, accepted 15 August 2008

## Abstract

Various deformation mechanisms may contribute to the high temperature plastic deformation of twin-roll cast AlMg3 (AA5754) sheets. The evaluation of the strain rate sensitivity parameter  $m$  suggested that grain boundary sliding, which is generally responsible for superplastic behaviour, might be operating at certain temperature and strain rate conditions. The investigation of the surface relief of samples strained at various deformation conditions was carried out using atomic force microscopy. Both grain boundary sliding and dislocation slip were observed. Grain boundary sliding was accompanied by intensive cavitation that prevented the material from reaching superplastic values of ductility.

**Key words:** AA5754 sheet, twin-roll casting, grain boundary sliding, atomic force microscopy, cavitation

## 1. Introduction

Aluminium sheets are usually manufactured from Direct Chill (DC) cast ingots by hot and cold rolling. Twin-Roll Continuous (TRC) casting is an alternative and cost efficient substitution for DC casting since the technology based on TRC does not involve the time and energy exigent hot rolling [1]. In spite of the indisputable ecological benefits of TRC, this technology is not widely used in the production of aluminium sheets for automotive applications. The main reason is the lack of experience in the down-stream processing and the limited knowledge of the properties of TRC sheets, especially in terms of their formability.

The ductility of aluminium sheets at room temperature is generally lower than 30 % [2], however, it can be improved by increasing the forming temperature [3, 4]. Al-Mg-based materials in particular exhibit large ductilities up to 300 % if strained at elevated temperatures [5, 6]. Such deformation behaviour usually results from a solute-drag controlled creep mechanism [7]. This deformation mechanism occurs even in coarse-grained materials. Simultaneously, it is well known that many Al-based sheet materials (including Al-Mg-based alloys) can exhibit superplastic be-

haviour if prepared with a fine-grained structure [8, 9]. Although both these types of deformation result in large ductility values, superplastic deformation is additionally characterized by a high strain rate sensitivity of the stress [10]. The high strain rate sensitivity parameter  $m = \partial \log \sigma / \partial \log \dot{\epsilon}$  (usually close to 0.5) suppresses the neck development during a tensile test and makes it possible to reach ductility values of many hundreds of percent. The grain size of the TRC AlMg3 alloy (AA5754) used in the present investigation is slightly below 10  $\mu\text{m}$  and might be, therefore, sufficient for superplastic behaviour.

Grain boundary sliding is believed to be the main deformation mechanism under superplastic conditions. This mechanism requires a simultaneous operation of accommodation mechanisms that remove the stress concentrations formed especially at triple points. In case of an insufficient rate of accommodation processes, internal cavities may be formed and the plasticity of the material is reduced in spite of the high strain rate sensitivity of the stress.

Our previous study of the TRC AA5754 alloy [11] based especially on the measurement of the parameter  $m$  and on the investigation of the deformation structure using light and atomic force microscopy resulted

\*Corresponding author: tel.: +420 221 911 363; fax: +420 221 911 490; e-mail address: [malek@met.mff.cuni.cz](mailto:malek@met.mff.cuni.cz)

into the following conclusions concerning the deformation mechanism operating under different deformation conditions:

- dislocation slip is the main mechanism at lower temperatures (473 K),
- a solute-drag controlled creep mechanism controls the deformation at elevated temperatures if the temperature compensated strain rate remains below a critical value [12],
- grain boundary sliding dominates at 723 K in a narrow range of strain rates close to  $10^{-4} \text{ s}^{-1}$  where superplastic characteristics were observed.

The main aim of the present investigation was to verify the forming potential of the TRC AA5754 material and to understand the microstructure development in specimens strained at various conditions. The images of the surface of strained samples were obtained using the Atomic Force Microscopy (AFM) method and critically discussed from the point of view of deformation mechanisms operating at different straining conditions.

## 2. Experimental

A twin-roll cast AA5754 alloy (2.69 Mg, 0.39 Mn, 0.31 Fe, 0.20 Si, all in wt.%) was used for the experiments. The TRC strip of 6 mm thickness was cold rolled to 1 mm and then annealed at 673 K for 10 minutes in order to prepare a fully recrystallized microstructure. The grains are slightly elongated along the rolling direction (about 10 %) and the mean grain size (determined as the mean intercept length) is approximately 8  $\mu\text{m}$  in the rolling direction.

Specimens for tensile testing ( $1 \times 8 \times 27 \text{ mm}$ ) were cut parallel to the rolling direction and strained both at room and elevated temperatures. The deformation temperatures and strain rates were chosen on the basis of the previous measurement of parameter  $m$ . The samples were strained to failure in order to determine the ductility.

In order to acquire information on the mechanism of plastic deformation, the surface relief of specimens strained at different conditions was examined using atomic force microscopy (AFM). The samples for these experiments were polished and then pulled up to elongations of 20 % and 40 %, respectively. The AFM investigation was carried out using an Explorer dry scanner Thermomicroscopes mostly on the area of  $100 \times 100 \mu\text{m}$ . For more detailed information the scanned area was reduced to  $20 \times 20 \mu\text{m}$ . Independently of the size of scanned area, each scan contained  $200 \times 200$  points where the height component was measured. The acquired digital data make it possible to reconstruct the surface relief either in the 3-dimensional (3-D) representation or in the form of images where different colours are attributed to places

with different slopes of the surface (internal sensor mode). In the latter case the places with the highest slope are represented by the extreme black or white colours. In order to quantify the surface relief, lines can be selected anywhere within the scanned area and the corresponding height profiles along these lines can be visualized.

The cavitation process was studied on the plane parallel to the rolling and short transversal directions. The specimens strained either to failure or to selected elongations were polished and studied with a light microscope. The images were processed using the LU-CIA image analysing system and the area fraction of cavities was evaluated.

## 3. Experimental results

The strain rate sensitivity parameter  $m$  is strongly dependent on the deformation conditions (Fig. 1). Its value is negligible at room temperature and remains very low up to 473 K within the entire range of strain rates studied. The value of  $m$  close to 0.3 (which is typical for a solute-drag controlled creep mechanism) was found at temperatures above 573 K. The range of strain rates corresponding to  $m$  values close to 0.3 extends to higher strain rates with increasing temperature. The highest value of  $m = 0.4$  corresponding to superplastic behaviour was observed at temperatures of 723 K and 748 K at strain rates of the order of  $10^{-4} \text{ s}^{-1}$ .

Four sets of deformation conditions were selected for further experiments:

- A. temperature 295 K, strain rate  $4.3 \times 10^{-4} \text{ s}^{-1}$  (corresponding to  $m$  close to 0),
- B. temperature 473 K, strain rate  $4.3 \times 10^{-4} \text{ s}^{-1}$  (corresponding to  $m = 0.05$ ),

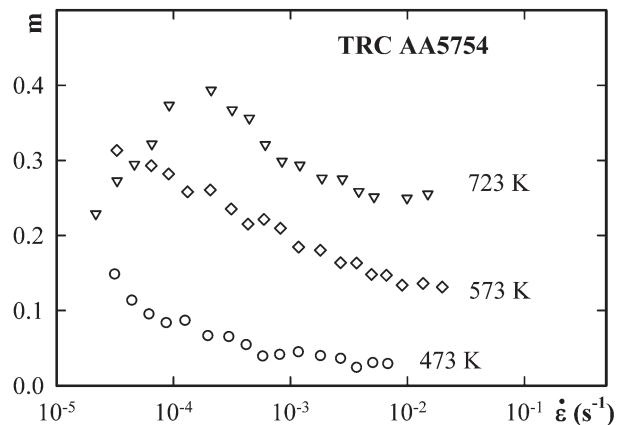


Fig. 1. The influence of temperature and strain rate on the strain rate sensitivity parameter  $m$ .

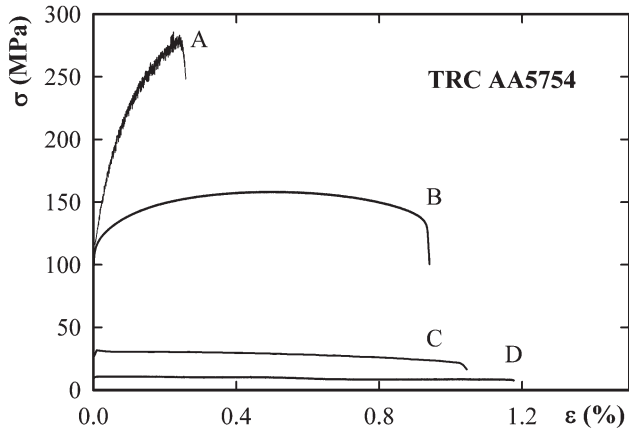


Fig. 2. The stress/strain curves for various deformation temperatures and strain rates: A. 295 K,  $4.3 \times 10^{-4} \text{ s}^{-1}$ , B. 473 K,  $4.3 \times 10^{-4} \text{ s}^{-1}$ , C. 723 K,  $1.9 \times 10^{-2} \text{ s}^{-1}$ , D. 723 K,  $4.3 \times 10^{-4} \text{ s}^{-1}$ .

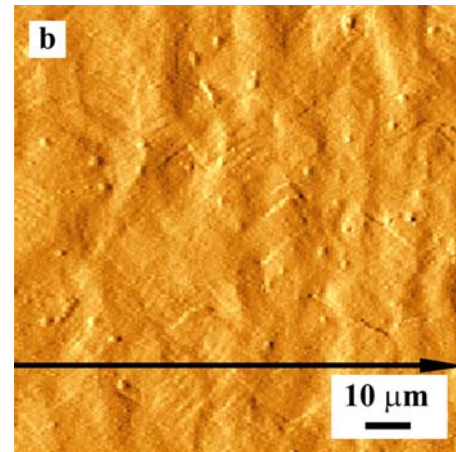
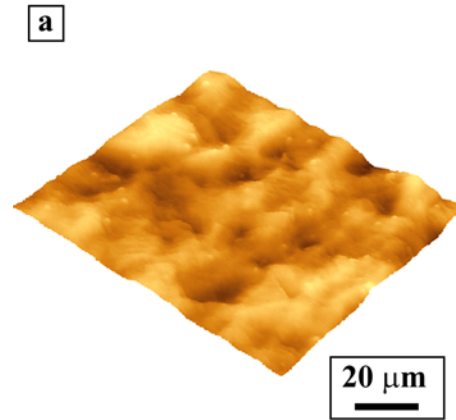
C. temperature 723 K, strain rate  $1.9 \times 10^{-2} \text{ s}^{-1}$  (corresponding to  $m = 0.25$ ),

D. temperature 723 K, strain rate  $4.3 \times 10^{-4} \text{ s}^{-1}$  (corresponding to  $m$  close to 0.4).

The results of tensile tests to failure at conditions A–D are given in Fig. 2. The increasing deformation temperature reduces the overall stress level and the strain hardening. The stress vs. strain curves exhibit a steady state character at 723 K. In spite of a remarkable difference in the parameter  $m$  values, similar values of ductility close to 100 % were observed at conditions B–D. The ductility remains deeply below the bottom limit of superplasticity even at conditions D where the parameter  $m = 0.4$  suggests superplastic behaviour.

Figures 3 and 4 compare the surface structure of samples strained to 20 % at conditions A and D both in the 3-D (a) and internal marker mode (b). The surface profiles along selected lines are given in part (c) of Figs. 3 and 4. It was found that the maximum height difference between the lowest and the highest points within the scanned area is similar in both samples: 1.9  $\mu\text{m}$  in sample A and 2.1  $\mu\text{m}$  in sample D. However, the character of the surface is quite different. The images from the sample strained at room temperature do not reveal individual grains and surface roughness results from a cooperative process – a number of valleys and ridges can be distinguished in the direction nearly parallel to the tensile direction. Regions containing many grains are inclined at the same angle to the original surface – see arrow in the surface profile. No steep slopes indicating grain boundary sliding were observed. Slip lines are present over the whole scanned area and the typical height step at the slip line is close to 100 nm. Similar surface structure was also observed on sample B, strained at 473 K.

The surface of sample D, strained at 723 K, and



height ( $\mu\text{m}$ )

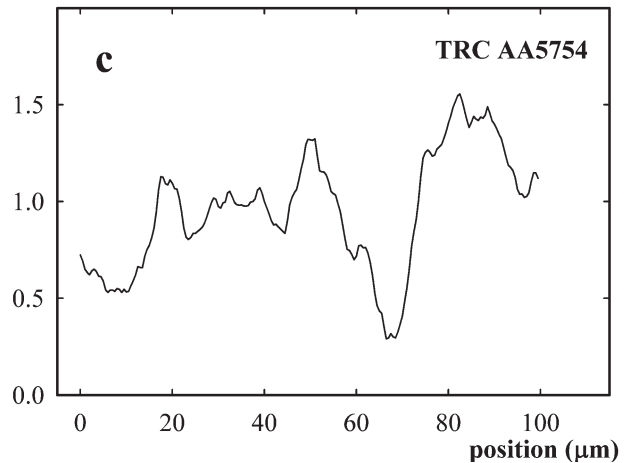


Fig. 3. The surface of the sample A strained to 20 % at 295 K/ $4.3 \times 10^{-4} \text{ s}^{-1}$  (tensile direction vertical): a) 3-D mode, b) internal marker mode, c) surface profile.

the strain rate corresponding to the maximum parameter  $m$  value is quite different and documents clearly the displacement of individual grains. Steep slopes of profiles in Fig. 4c suggest that grain boundary sliding occurs at the majority of boundaries (profile 1)

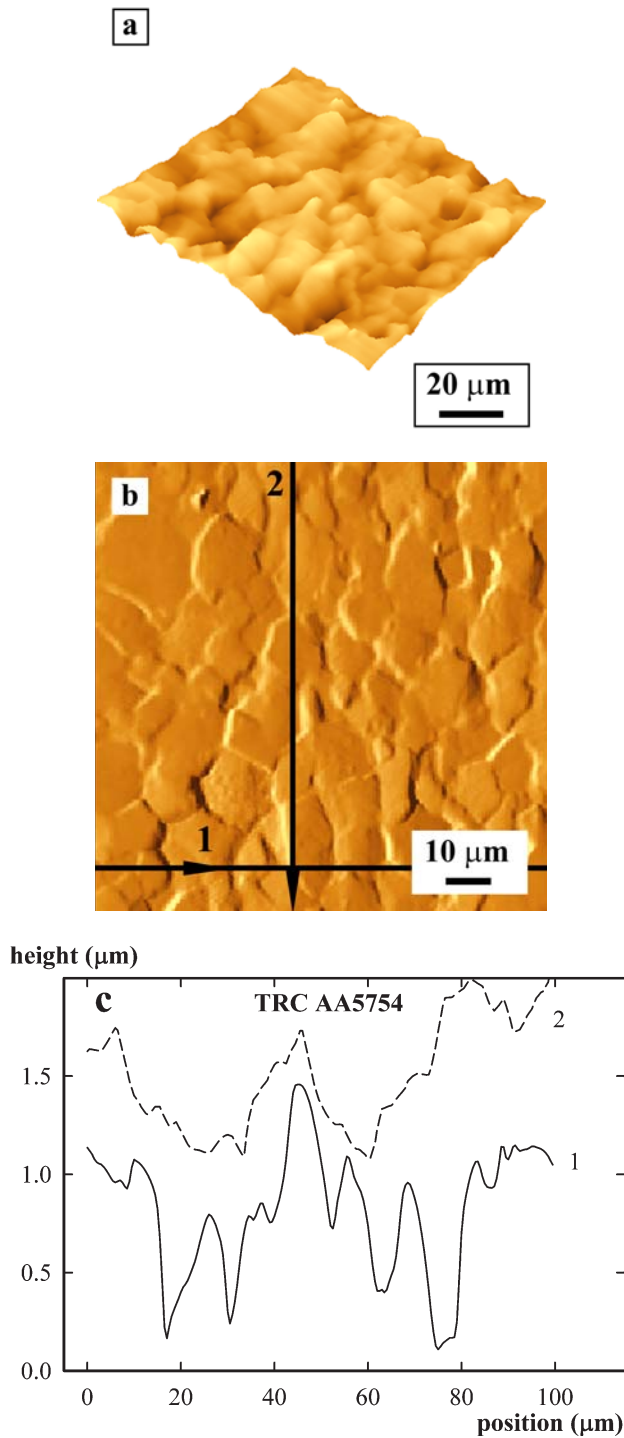


Fig. 4. The surface of the D sample strained to 20 % at 723 K/ $4.3 \times 10^{-4} \text{ s}^{-1}$  (tensile direction vertical): a) 3-D mode, b) internal marker mode, c) surface profiles.

and the height of steps at grain boundaries is usually between 500 and 1000 nm. This size corresponds to approximately 10 % of the grain size. A much lower frequency of large steps was observed at boundaries perpendicular to the tensile axis (profile 2).

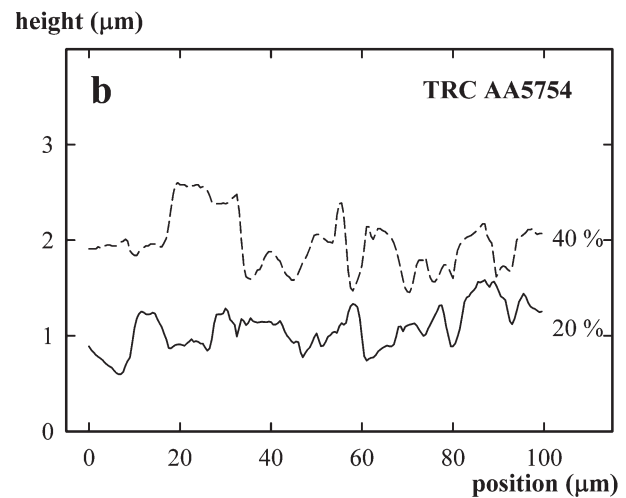
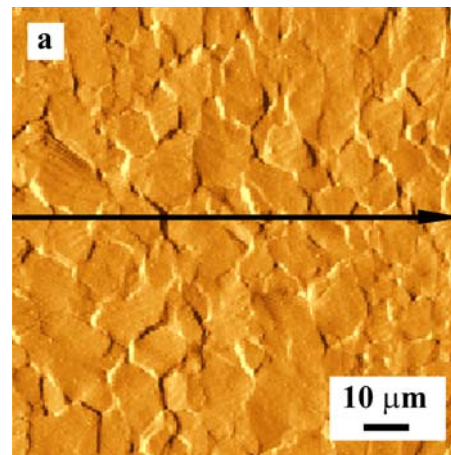


Fig. 5. The surface of the sample C strained to 40 % at 723 K/ $1.9 \times 10^{-2} \text{ s}^{-1}$  (tensile direction vertical): a) internal marker mode, b) surface profiles for elongation of 20 and 40 %.

The measurement of parameter  $m$  documents clearly that the deformation mechanism at 723 K also depends on the strain rate (see  $m$ -values for samples C and D). Figures 5a and 6a compare the surfaces of samples strained at conditions C and D to the elongation of 40 %. Mutual shifts of most grains were observed in both samples. However, the surface profiles show the great difference between the magnitudes of these shifts (Figs. 5b and 6b). Whereas the maximum shifts of grains remain below 1 μm in the sample C strained at high (non-superplastic) strain rate, values exceeding 2 μm were found at many grain boundaries in the sample D strained at low (superplastic) strain rate. Moreover, Figs. 5b and 6b show the comparison of surface profiles taken from samples strained to 40 and 20 %, respectively. The profiles measured at non-superplastic conditions C show only a slight increase in the mean sliding distance if the sample elongation is doubled from 20 to 40 %. A significantly

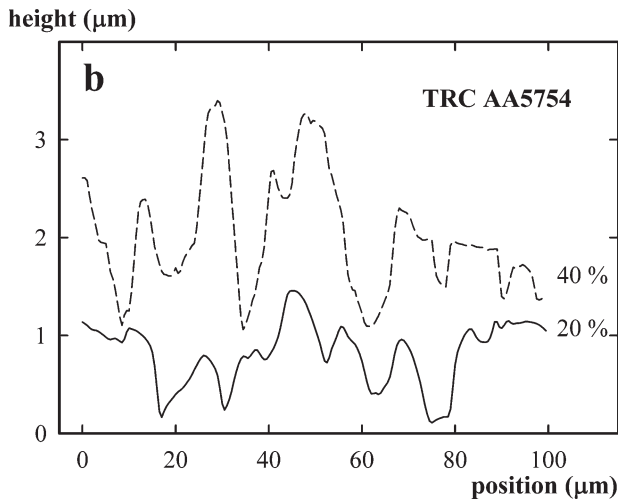
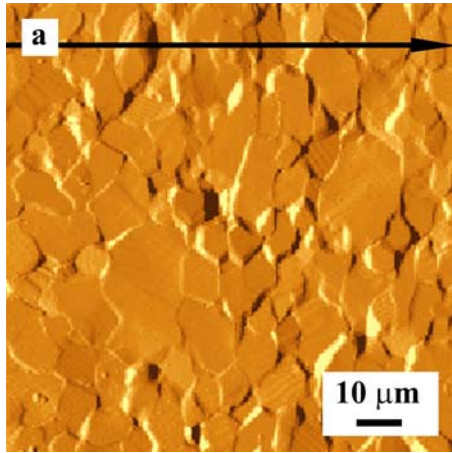


Fig. 6. The surface of the sample D strained to 40 % at 723 K/ $4.3 \times 10^{-4} \text{ s}^{-1}$  (tensile direction vertical): a) internal marker mode, b) surface profiles.

more pronounced influence of sample elongation on the sliding distance was observed at superplastic deformation conditions D. The increase in the sliding distance seems to be proportional to the increase in the sample elongation.

A detailed inspection of AFM micrographs obtained from samples elongated to 40 % shows the presence of slip lines in the interior of many grains. This phenomenon is more pronounced in the sample strained at non-superplastic conditions C, however, individual grains containing slip lines were also observed in the sample strained at superplastic conditions D. A group of neighbouring grains containing slip lines is shown in Fig. 7 for the sample strained at superplastic conditions.

Figure 7 offers the possibility to compare the surface roughness resulting from grain boundary sliding and dislocation slip, respectively. The surface profile in the direction perpendicular to slip lines (along a line marked in Fig. 7) shows that the height of individual

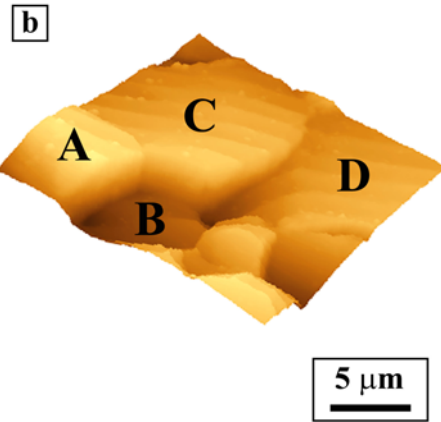
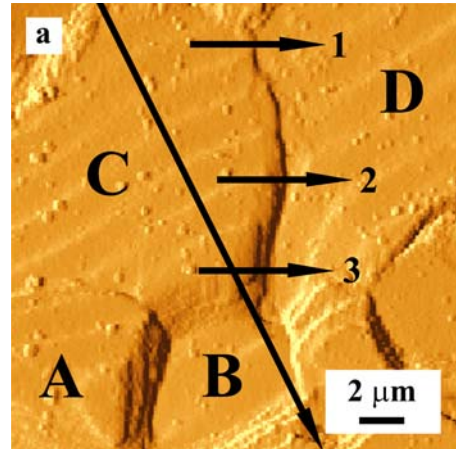


Fig. 7. The surface of the sample D strained to 40 % at superplastic conditions (tensile direction vertical): a) internal marker mode, b) 3-D mode.

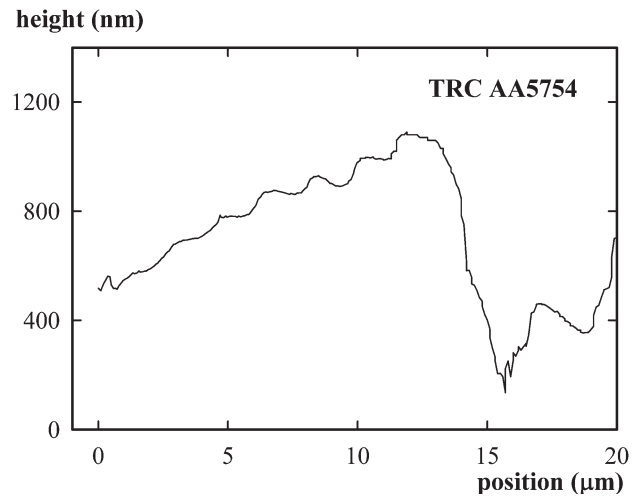


Fig. 8. Surface profile along the line marked in Fig. 7, perpendicular to the slip lines.

slip steps is of the order of 100 nm, whereas the shifts of neighbouring grains due to grain boundary sliding

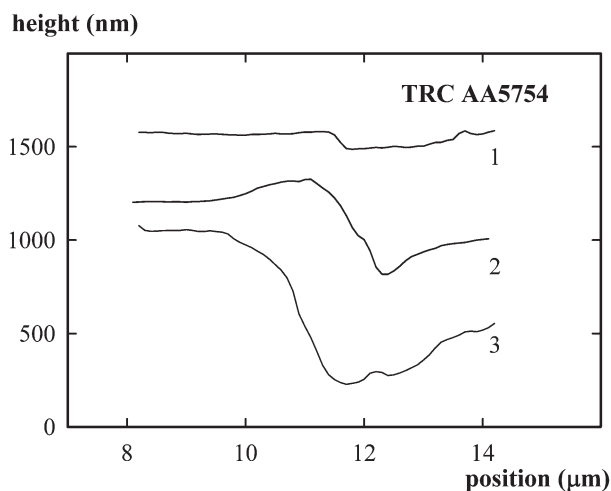


Fig. 9. Surface profiles across the boundary between grains C and D in Fig. 7 at various places.

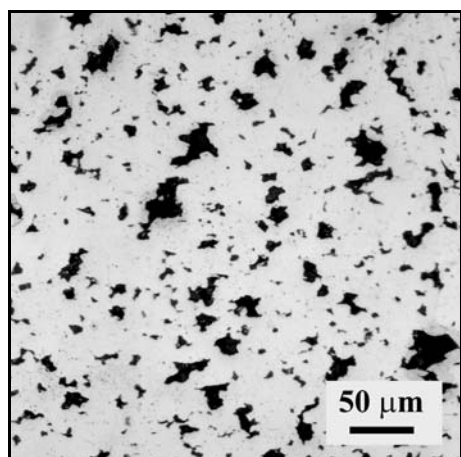


Fig. 10. Cavitation in the sample D strained to failure at superplastic conditions, tensile axis horizontal.

are one order of magnitude larger (Fig. 8). Additionally, the detailed insight into the surface of strained samples yields a very important conclusion concerning the origin of mutual grain displacements. The displacement between grains A and B in Fig. 7 results from grain boundary sliding. On the other hand, dislocation slip occurring in grain C results in the rotation of this grain and, consequently, in the displacement between grains C and D. Profiles taken at different places (1 to 3) across the boundary between grains C and D confirm this rotation – the displacement of grains C and D along their common boundary increases from place 1 to 3 (Fig. 9).

The AFM micrographs taken from the sample strained to 40 % at conditions D (723 K,  $4.3 \times 10^{-4} \text{ s}^{-1}$ ) reveal the formation of cavities at triple points (see e.g. the 3-D image in Fig. 7). In order to verify the occurrence of this process, several samples were

Table 1. Cavity area fraction in the sample D strained to various elongations

Elongation (%)	14	40	80	120 (rupture)
Cavity area fraction (%)	1.8	2.3	11	16

strained at conditions D to various elongations and the area fraction of cavities was evaluated. The results of this experiment summarized in Table 1 show that the cavity area fraction starts to increase at elongation higher than 40 % and reaches remarkably high values at fracture strain. The light micrograph of sample D strained to fracture (elongation of approximately 120 %) in Fig. 10 shows a homogeneous distribution of cavities without any elongation along the tensile axis. The size of the largest cavities exceeds the mean grain size.

#### 4. Discussion

The results of tensile tests to rupture confirmed the expected increase in formability with increasing temperature. The significant ductility increase was observed already at 473 K and correlates well with the decrease in strain hardening. It can be expected that the motion of lattice dislocations represents the main deformation mechanism both at 295 and 473 K. The differences in the deformation behaviour at these temperatures reflect the increasing role of restoration processes at 473 K.

The stress-strain curves obtained at 723 K are very similar independently of the strain rate used. Both curves exhibit negligible strain hardening so that certain models of steady state creep can be used for the explanation of the deformation behaviour. Despite the similar ductility values, it was concluded in our previous paper [11] that a solute-drag controlled creep mechanism based on the slip of lattice dislocations in the atmosphere of solute atoms was dominating at higher strain rates (conditions C) and a superplastic mechanism based on grain boundary sliding was suggested as the dominating mechanism at lower strain rates (conditions D).

The investigation of the surface roughness of samples strained at different conditions (A to D) using the AFM method was used to confirm the above-mentioned hypotheses. AFM is a powerful tool for the quantitative assessment of the deformation mechanism under various straining conditions. The investigations of surface topography using AFM after fatigue [13, 14], indentation tests [15] or tensile tests [9, 11, 16] are still relatively scarce. However, the importance of AFM will increase as it yields very precise quant-

ative data on the height of slip bands and on the displacements of neighbouring grains along their common boundary during grain boundary sliding. The high accuracy in the determination of the vertical coordinate simultaneously with the high lateral resolution make it possible to investigate the deformation mechanism even in modern microcrystalline or submicrocrystalline materials [17, 18].

The present AFM investigation of the TRC AA5754 alloy revealed a similar surface roughness of samples strained both at low and high temperatures – see the surface profiles in Figs. 3c and 4c. However, the source of this roughness is quite different. Rotations of grain groups due to dislocation slip and numerous slip lines with the height of individual slip steps up to 100 nm are typical for low temperature deformation. Distinct grain boundaries and grain displacements reaching nearly 1  $\mu\text{m}$  are typical for the deformation at 723 K. A detailed evaluation of AFM images revealed a broad distribution of grain displacements at various boundaries. This distribution cannot result from the diversity in misorientation angles of individual boundaries, as a preliminary EBSD investigation revealed that most boundaries present in the initial state are general high-angle boundaries, which are suitable for GBS. The size of grain displacements is thus determined especially by the orientation of individual grain boundaries to the tensile direction (TD). This explanation is supported by the observation of a significantly lower amount of GBS along boundaries perpendicular to TD.

The AFM images obtained from samples strained at 723 K at conditions C and D show distinct boundaries, i.e. the operation of GBS both at low (superplastic) and high (non-superplastic) strain rates (Figs. 5 and 6). Nevertheless, the comparison of grain displacements in both samples reveals a higher contribution of GBS to the total strain on superplastic conditions. On the other hand, slip lines observed in the interior of most grains in Fig. 5 confirm that dislocation slip contributes significantly to the strain at non-superplastic (C) conditions. The frequency of grains containing slip lines is much lower in the sample strained on superplastic conditions (D), i.e. the contribution of dislocation slip is lower. Both mentioned deformation mechanisms are interconnected. The models of superplastic deformation suppose that GBS must be accompanied by other mechanisms removing stress concentrations at triple points or other obstacles for sliding. Dislocation slip is considered as one of the most probable accommodation mechanisms [10]. Our AFM investigation revealed the opposite relationship as well – dislocation slip in the grain interior results in the rotation of this grain with respect to the neighbouring one and, consequently, a grain displacement can be observed.

The high contribution of GBS to the total strain and the high value of the parameter  $m$  under conditions D should be good prerequisites for achieving a high ductility. Unfortunately, this is not the case in the studied TRC AA5754 alloy. The ductility remains deeply below the limit of superplasticity and does not differ significantly from that found at non-superplastic conditions C. Similarly to results obtained for the continuously cast Al-Mg alloy [19], cavitation can be the reason for premature failure. Table 1 shows a very high fraction of cavities in the sample strained to rupture on superplastic conditions D (0.16). The cavitation process starts at early stages of straining but its rate increases at strains higher than 40 %. Figure 7b shows that cavities are initially formed at triple points but their size gradually increases up to dimensions exceeding the grain size. It can be supposed that cavitation is a consequence of an imperfect accommodation of GBS. This conclusion is supported by the finding of significantly weaker cavitation in the sample strained at non-superplastic conditions C. In this case, the contribution of grain boundary sliding is lower, and the area fraction of cavities in the fractured sample reaches only 0.034.

#### 4. Conclusions

The ductility of the twin-roll cast AA5754 alloy close to 100 % was observed at temperatures above 473 K. The ductility values do not correlate with the value of strain rate sensitivity parameter  $m$ .

Dislocation slip is the main operating deformation mechanism at 295 and 473 K. Grain boundary sliding contributes strongly to the total strain at 723 K. Larger grain displacements and a lower activity of dislocation slip were observed at conditions D corresponding to the superplastic value of the parameter  $m$ .

AFM makes it possible to obtain quantitative data on the height of slip steps and grain displacements during GBS.

Cavitation resulting from an imperfect accommodation of GBS is the reason for premature failure at superplastic conditions D.

#### Acknowledgements

The authors would like to dedicate the paper to Professor Michael Boček on the occasion of his 80th birthday.

The authors are grateful to Ing. I. Drbohlav, Institute of Physics, Acad. of Sciences, Prague and to A. Aimoz, INP, ENSEEG Grenoble for their participation in the various experiments. This work is a part of the research project 1M 2560471601 financed by the Ministry of Education, Youth and Sports of the Czech Republic. AL INVEST Břidličná kindly supplied the input material.

## References

- [1] HAMER, S.—TARAGLIO, B.—ROMANOWSKI, C.: *Light Metal Age*, Oct., 2002, p. 6.
- [2] LI, D.—GHOSH, A.: *Mat. Sci. Eng. A*, 352, 2003, p. 279.
- [3] AYRES, R. A.—LANNING, H. W.—TAYLOR, B.—HEIMBUCH, R.—BRAZIER, W. G.: SAE Paper 780180, Society of Automotive Engineers, 1978, p. 702.
- [4] AYRES, R. A.—WENNER, M. L.: *Metall. Trans.*, 10A, 1979, p. 41.
- [5] WOO, S. S.—KIM, Y. R.—SHIN, D. H.—KIM, W. J.: *Scripta Mater.*, 37, 1997, p. 1351.
- [6] TALEFF, E. M.—HENSHALL, G. A.—NIEH, T. G.—LESUER, D. R.—WADSWORTH, J.: *Met. Mater. Trans.*, 29A, 1998, p. 1081.
- [7] McQUEEN, H. J.—KASSNER, M. E.: In: *Superplasticity in Aerospace*. Eds.: Heikkinen, H. C., McNelley, T. R. Warrendale, TMS 1988, p. 77.
- [8] TURBA, K.—MÁLEK, P.—CIESLAR, M.: *Kovove Mater.*, 45, 2007, p. 165.
- [9] MÁLEK, P.—CIESLAR, M.—BARTUŠKA, P.—DRBOHLAV, I.: *Kovove Mater.*, 43, 2005, p. 1.
- [10] EDINGTON, J. W.—MELTON, K. N.—CUTLER, C. P.: *Prog. Mater. Sci.*, 21, 1976, p. 61.
- [11] MÁLEK, P.—TURBA, K.—SLÁMOVÁ, M.—DRBOHLAV, I.: *Mater. Charact.*, 58, 2008, p. 1046.
- [12] McNELLEZ, T. R.—MICHEL, D. J.—SALAMA, A.: *Scripta Met.*, 23, 1989, p. 1657.
- [13] GERBERICH, W. W.—HARVEY, S. E.—KRAMER, D. E.—HOEHN, J. W.: *Acta Mater.*, 46, 1998, p. 5007.
- [14] VILLECHAISE, P.—SABATIER, L.—GIRARD, C.: *Mater. Sci. Eng. A*, 323, 2002, p. 377.
- [15] SPANL, M.—PÜSCHL, W.—SPRUŠIL, B.—ŠACHL, J.—ŠÍMA, V.—PFEILER, W.: *Mater. Trans*, 43, 2002, p. 560.
- [16] HUANG, Y.—LANGDON, T. G.: *J. Mater. Sci.*, 37, 2002, p. 4993.
- [17] MÁLEK, P.—TURBA, K.—CIESLAR, M.—DRBOHLAV, I.—KRUMML, T.: *Mater. Sci. Eng. A*, 462, 2007, p. 95.
- [18] CHINH, N. Q.—SZOMMER, P.—HORITA, Z.—LANGDON, T. G.: *Adv. Mater.*, 18, 2006, p. 34.
- [19] KULAS, M.-A.—GREEN, W. P.—TALEFF, E. M.—KRAJEWSKI, P. E.—McNELLEY, T. R.: *Met. Mater. Trans. A*, 37, 2006, p. 645.